USCAP

Check for updates

TECHNICAL REPORT

Patient-derived xenografts and in vitro model show rationale for imatinib mesylate repurposing in HEY1-NCoA2-driven mesenchymal chondrosarcoma

Polona Safaric Tepes [1,2,6 ✉], Danilo Segovia[1,3], Sania Jevtic[4], Daniel Ramirez[5], Scott K. Lyons[1] and Raffaella Sordella[1,6]

Mesenchymal chondrosarcoma (MCS) is a high-grade malignancy that represents 2–9% of chondrosarcomas and mostly affects children and young adults. HEY1-NCoA2 gene fusion is considered to be a driver of tumorigenesis and it has been identified in 80% of MCS tumors. The shortage of MCS samples and biological models creates a challenge for the development of effective therapeutic strategies to improve the low survival rate of MCS patients. Previous molecular studies using immunohistochemical staining of patient samples suggest that activation of PDGFR signaling could be involved in MCS tumorigenesis. This work presents the development of two independent in vitro and in vivo models of HEY1-NCoA2-driven MCS and their application in a drug repurposing strategy. The in vitro model was characterized by RNA sequencing at the single-cell level and successfully recapitulated relevant MCS features. Imatinib, as well as specific inhibitors of ABL and PDGFR, demonstrated a highly selective cytotoxic effect targeting the HEY1-NCoA2 fusion-driven cellular model. In addition, patient-derived xenograft (PDX) models of MCS harboring the HEY1-NCoA2 fusion were developed from a primary tumor and its distant metastasis. In concordance with in vitro observations, imatinib was able to significantly reduce tumor growth in MCS-PDX models. The conclusions of this study serve as preclinical results to revisit the clinical efficacy of imatinib in the treatment of HEY1-NCoA2-driven MCS.

INTRODUCTION

Mesenchymal chondrosarcoma (MCS) is a rare and aggressive subtype of chondrosarcoma that presents a paradigmatic advance of precision medicine in rare tumor diagnosis[1]. Before the discovery of the recurrent HEY1-NCoA2 gene fusion, the tumor presented a diagnostic challenge due to its histopathological similarities to many other small round blue cell tumors[2–4]. The identification of HEY1-NCoA2 gene fusion in 2012 led to diagnostic modifications using this fusion as a novel biomarker to unequivocally diagnose MCS[5,6].

MCS mostly affects children and young adults[1]. Despite advancements in diagnosis, radical surgical resection is still the mainstay of MCS management, which is typically followed by systemic therapy using different chemotherapy regimens[7,8]. The 10-year survival rate of MCS varies from 27 to 43%, with over half of MCS patients experiencing a relapse with local or distant metastases[8–10]. Yet, the use of conventional chemotherapy regimens and/or radiotherapy seems to have no benefit to the event-free survival rate of MCS patients[8,9].

In addition to the shortfall of effective treatment, our understanding of the molecular biology of HEY1-NCoA2 fusion-driven MCS is very limited. HEY1 is a transcriptional repressor and member of the basic helix-loop-helix (bHLH) protein family that

stimulates chondrocyte maturation[11,12]. NCoA2 is a member of the p160 transcriptional coactivator family that is activated by ligand-dependent nuclear receptors with the ability to modify chromatin structure and promote transcription[13,14]. In the HEY1-NCoA2 oncoprotein, the amino-terminal bHLH-DNA binding domain of HEY1 is retained and fused to the carboxy-terminal domain of NCoA2, transforming the fusion into a potent transcriptional activator[1,15,16]. Due to the large intrinsically disordered regions of NCoA2, lacking hydrophobic pockets where small molecules can bind, the HEY1-NCoA2 oncoprotein is so far considered undruggable[17–20].

The bulk of current knowledge on the topic of molecular signaling pathways involved in MCS tumorigenesis mostly relies on a few immunohistochemical (IHC) staining studies with limited amounts of patient samples and unknown fusion status. In MCS tumors, the overexpression or activation of PKC-α, PDGFR-α, antiapoptotic Bcl-2, mTOR, FGFR3, SOX9, and JNK signaling pathways was observed, indicating their potential role in the development or maintenance of MCS tumorigenesis[21–25]. The authors of these studies suggested the use of therapies targeting either the mTOR pathway, such as rapamycin, or PDGFR inhibitors such as imatinib mesylate (imatinib)[22,23]. A more recent study using a MCS-derived cell line, MCS170, showed a reduction in cell

[1]Cold Spring Harbor Laboratory, 1 Bungtown Road, Cold Spring Harbor, NY 11724, USA. [2]Faculty of Pharmacy, University of Ljubljana, Kongresni trg 12, 1000 Ljubljana, Slovenia. [3]Graduate Program in Molecular and Cellular Biology, Stony Brook University, 100 Nicolls Rd, Stony Brook, NY 11794, USA. [4]Phytoform Labs Ltd., Lawes Open Innovation Hub, West Common, Harpenden, Hertfordshire, England, UK. [5]Hospital for Special Surgery, Pathology and Laboratory Medicine, 535 E 70th St, New York, NY 10021, USA. [6]These authors contributed equally: Polona Safaric Tepes, Raffaella Sordella. ✉email: safaric.tepes@gmail.com

viability when cells were treated with a combination of the BH3 mimetic ATB-737 (targeting antiapoptotic BCL-2) and doxorubicin or cisplatin, while single treatment with ATB-737 showed no significant effect, suggesting that ATB-737 could sensitize the MCS to chemotherapy[26].

In this work, traditional and modern laboratory techniques[27] were complemented with a drug repurposing strategy to find clinically available drugs for MCS management. An in vitro model of MCS was developed and a molecular characterization at the single-cell mRNA level (sc-RNA) was performed. In addition, novel in vivo models of HEY1-NCoA2 fusion-driven MCS derived from a primary tumor and its distant metastasis were generated. Clinically available imatinib was identified as a highly selective cytotoxic agent targeting these new MCS models. These promising results could lead to a rapid translation into confirmatory clinical studies.

MATERIALS AND METHODS

Cell reagents and antibodies
Frozen vials of primary human articular chondrocytes (human primary chondrocytes (HPC)) were obtained from Cell Applications (San Diego, CA, USA, cat#402-05a). The following antibodies were used for immunoblotting (1:1000 dilution): HEY1 (Invitrogen, San Diego, CA, USA, cat#PA5-42008), NCoA2/SRC2 (Invitrogen, cat#PA5-29482), Flag-tag (Abcam, Cambridge, MA, USA, cat#ab213519), FGFR1 (Abcam, cat #ab76464), Col2A (Abcam, #ab188570), PDGFR-α (Abcam, cat#ab96569), PDGFR-β (Proteintech, Rosemont, IL, USA, cat#13449-1-AP), AXL (Cell Signaling Technology Inc., Danvers, MA, USA, cat#8661), and ABL1/2 (MyBioSource, San Diego, CA, USA, cat#MBS820417). The same ABL1/2 antibody was used for IHC staining. Antibody β-tubulin (Thermo Fisher, Waltham, MA, USA, cat#32-2600), was used in 1:3000 dilution.

For competition assays, the following drugs were obtained from Selleckchem (Houston, TX, USA): imatinib mesylate (cat#S1026), rapamycin (cat#S1039), regorafenib (cat#S4947), CP-673451 (cat#S1536), JNK-IN-8 (cat#S4901), asciminib (cat#S8555), doxorubicin (cat#S1208), and cisplatin (cat#S1166).

Culture of HPC
HPC vials were thawed according to the manufacturer's instructions into T25 flasks, incubated at 2% oxygen in either commercially available chondrocyte growth media (Cell Applications, cat#411-500; PromoCell, Heidelberg, Germany, cat#C-27101; ChondroLife, Lifeline Cell Technology, Walkersville, MD, USA, cat#LM-0022), or media developed in our laboratory, chondrocyte induction media (CIM). CIM consisted of DMEM GlutaMAX (Thermo Fisher), 1% ITS (insulin, transferrin, selenous acid) solution (Sigma Chemical, St. Louis, MO, USA), 1% nonessential amino acids (Sigma Chemical), 1.25 mg/ml human serum albumin (Thermo Fisher), 5 ng/ml FGF (R&D Systems, Minneapolis, MN, USA), 5 ng/ml PDGF-BB (Millipore, Burlington, MA, USA), 20 mM HEPES pH 7.5 (Sigma Chemical), and 1 mM sodium pyruvate (Sigma Chemical). CIM was selected as the best HPC culturing media and was used for further manipulations of HPC. Cells were passaged approximately every 3 days or when they reached 80% density.

Growth rate and population doubling of HPC
A total of 12 vials of cryopreserved adult HPC (Cell Application, cat#402-05a) were thawed and cultured using different media with culturing conditions described in the previous section. Each vial contained 5×10^5 adult HPC and was plated in separated T25 flasks. Cells were counted by an automated cell counter four times using trypan blue. The number of cells at the end of each passage was recorded for each tested media. Population growth rate and population doubling time (PDT) were calculated and plotted using GraphPad Prism. The growth rate was calculated as Growth Rate (cells/cm²/days) = [(Ne/Ns)/surface area/d], where Ne is the cell count at the end, Ns is the cell count at the beginning of the passaged cell culture, and d is duration of culture in days. PDT was calculated as PDT (days) = [Nt/Nd], where Nt is time the cells were in the culture (days) and Nd is doubling number in each passage with formula: Nd = Log[Ne/Ns]/Log2.

Construction of expression plasmid
The HEY1-NCoA2 gene fusion was designed with an in-frame Flag-tag on the 5′ end and P2A-mVenus on the 3′ end and submitted for gene synthesis to Genscript. The Flag-tag-HEY1-NCoA2-P2A-mVenus sequence was cloned into a Gateway Donor Vector. By using the Gateway cloning system, the insert in the Donor Vector was transferred in an LR reaction to the Destination Vector pLenti CMV Puro Dest (Addgene, Watertown, MA, USA, cat#17452). The plasmid pLenti CMV Puro Dest eGFP (Addgene, cat#107505) was used as a vector control (Fig. 1a). All constructs were subsequently analyzed by Sanger sequencing.

Lentiviral production and infection
To produce VSV-G pseudotyped lentivirus (LV) we cotransfected three plasmids into HEK293FT cells. Briefly, 6×10^6 293FT cells were seeded onto 10 cm² plates. Twenty-four hours later, the cells were transfected with the second generation LV packaging plasmids: psPAX2 (6 μg), pMD2.G (VSV-G expression plasmid) (3 μg), and pLenti CMV Puro Dest-HEY1-NCOA2 (10 μg) or pLenti CMV Puro Dest eGFP (10 μg), using lipofectamine 2000 (Invitrogen, cat# 11668019). The media were changed after 24 h, and LV media were collected 48 h after transfection. Following collection, LV media were passed through 0.45 μm filter and used immediately. LV was prepared fresh for each transduction.

Primary cells transduction and lentiviral titration
For HPC transduction, 1×10^6 cells were seeded in T75 flasks. After 48 h, the cells were infected with 10 ml of LV media supplemented with 10 μg/ml of polybrene reagent (Sigma-Aldrich, St. Louis, MO, USA, cat#TR-1003). Forty-eight hours later, the media were changed to CIM media. Seventy-two hours later, the percentage of GFP or mVenus expression (GFP+ cells) was measured using flow cytometry (Guava® easyCyte 11HT Benchtop Flow Cytometer, Millipore Sigma, Burlington, MA, USA) and analyzed with the GuavaSoft and FlowJo software package (Millipore Sigma). The functional titer of each LV preparation was determined by flow-cytometry analysis based on GFP+ measurements.

Cell competition assay
HPC at 70% density were infected with LV as described above to obtain an infection rate of ~50% GFP+ cells, as confirmed by flow cytometry (Guava, Millipore Sigma). Next, the cells were seeded in 12-well plates at a density of 0.5×10^6 cells per well. The percentage of GFP+ cells was measured by flow cytometry at four time points: on the day the cells were plated, day 2, day 5, and day 8 after seeding (in triplicates) and analyzed by GuavaSoft program. The experiment was repeated four times. GraphPad Prism was used for statistical analysis. The significance of an increase or decrease in GFP+ cells was assessed by two-way ANOVA multiple comparisons where each day was compared to day 0 ($p \leq 0.05$ was considered as significant). The significant change in proliferation between HPC expressing HEY1-NCoA2 and vector control on day 8 was calculated by the two-tailed Student's t test ($p \leq 0.05$ was considered as significant).

Single-cell captures, library preparation, and RNA sequencing
Single-cell suspension of HPC was washed and resuspended in PBS containing 0.04% BSA. Cells were counted on Countess II automated cell counter (Thermo Fisher), and up to 12,000 cells were loaded per lane on 10X Chromium microfluidic chips. Single-cell capture, barcoding, and library preparation were performed using the 10X Chromium version 2 chemistry (10X Genomics, Pleasanton, CA, USA, Single Cell 3′ Library Gel Bead Kit V2), and according to the manufacturer's protocol (10X Genomics, cat#CG00052). cDNA libraries were checked for quality on Agilent 4200 Tapestation and quantified by KAPA qPCR before sequencing on a single lane of a HiSeq4000 (Illumina, San Diego, CA, USA) to an average depth of 50,000 reads per cell with a paired-end 150 bp reading strategy.

Single-cell data processing, quality control, and analysis
The Cell Ranger pipeline (10X Genomics, v1.3) was used to convert Illumina base call files to FASTQ files, align FASTQs to the hg19 reference (10X Genomics, v1.2.0) for human samples, and to produce a digital gene-cell count matrix. Samples were combined using the Cell Ranger aggregate function, which subsamples digital counts matrices such that the number of confidently mapped transcriptomic reads is equal among all samples and creates a unified digital count matrix. Clustering was performed with scanpy (a single-cell gene expression analysis library written in python)[28]. Gene-cell count matrices were filtered in such manner that the cells that followed these criteria were removed: the cells with a gene number < 200, cells with gene number ranked in the top 1%, and cells with a
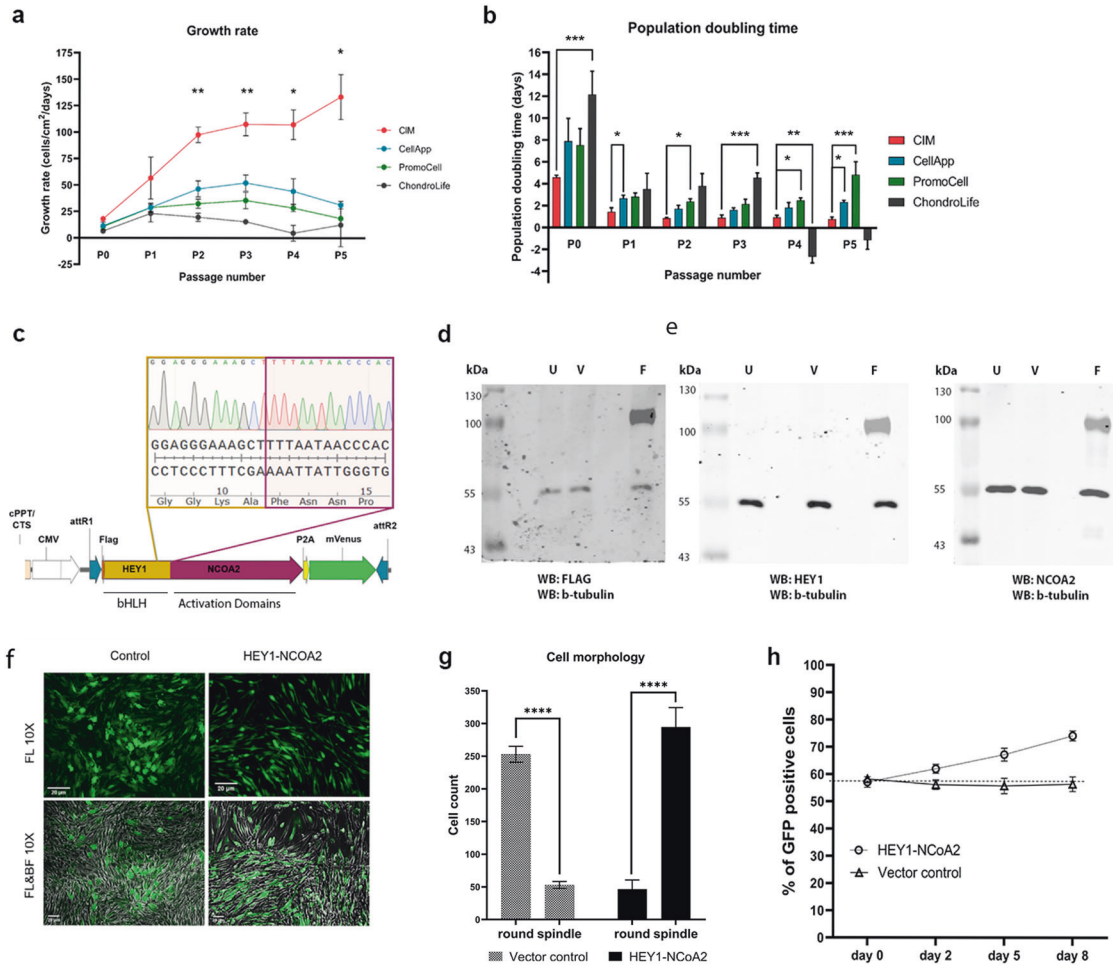
Fig. 1 HEY1-NCoA2 expressing human primary chondrocytes show a growth advantage and morphology changes. a The calculated growth rate for HPC in different media up to P5. Asterisks denote significant changes (*$p < 0.05$, **$p < 0.01$, two-way ANOVA test, $N = 3$). **b** Calculated population doubling time of HPC in different media up to P5. Asterisk marks significant changes (*$p < 0.03$, **$p < 0.01$, ***$p < 0.005$, ****$p < 0.001$, two-way ANOVA test, $N = 3$). **c** Schematic representation of the construct used to transduce HPC. Flag-tag-HEY1-NCoA2 gene fusion is expressed under CMV promoter together with the traceable marker mVenus, which is separated by the 2A self-cleavage peptide. HEY1 has conserved bHLH domain in the fusion, while NCoA2 has conserved its activation domains. **d, e** Western blot analysis of untransduced HPC (U), vector control (V), or fusion transduced (F) HPC. Specific Flag-tag, HEY1, and NCoA2 antibodies recognized a 100 kDa protein. β-tubulin was used as a loading control. **f** Representative fluorescent microscopy images of HEY1-NCoA2-HPC or vector control-HPC. **g** The graph is depicting the average cell count for spindle-shaped cells and round cells in three different fields of three independent experiments in HEY1-NCoA2-HPC or Vector control-HPC (****$p < 0.0005$, Student's paired t test, $N = 3$). **h** The fluorescence cell competition assay plot shows the percentage of GFP+ or mVenus+ HPC over time as determined by flow cytometry. HEY1-NCoA2-HPC presented a growth advantage as compared to vector control-HPC (ANOVA test, $p < 0.0001$, $N = 5$).

mitochondrial gene ratio of >25%. The gene-cell count matrices were then normalized such that the number of unique molecular identifiers (UMI) in each cell was equal to the median UMI count across the data set and log-transformed. Dimensionality reduction was performed using principal component analysis), and t-distributed stochastic neighbor embedding and uniform manifold approximate and projection (UMAP) were used for further dimensionality reduction and visualization.

Gene set enrichment analysis (GSEA)
HPC expression profiling files were analyzed by GSEA. GSEA was performed using the GSEA v2.0.13 software. All gene set files for this analysis were obtained from the GSEA website (www.broadinstitute.org/gsea/). An enrichment map was used for visualization of the GSEA results.

Fluorescence competition assay for drug screening
HPC were infected with LV at 70% density as described above to obtain an infection rate of ~50% of GFP+ cells (analyzed by flow cytometry). Next, the cells were seeded in 96-well plates at a density of 2500 cells per well. After 24 h the different concentrations of drugs were added, using automated drug dispenser Tecan HP D300e Digital Dispenser. After 72 h,

the cells were detached with TrypLe (Gibco, TX, USA, cat#12605036) and GFP ratio was measured using flow cytometry (Guava, Millipore Sigma) and results were analyzed using the GuavaSoft software package and FlowJo. The percentage of GFP+ cells and the number of total cells in the well were measured by Guava easyCyte. Each point represents the average of six independent biological replicates. Drug assays were repeated 3–5 times in independent experiments, where LV was each time freshly prepared. In the control plates, only DMSO was added in concentrations, that correspond to the percentage of the DMSO in the diluted drug, which was calculated by automated drug dispenser Tecan HP D300e Digital Dispenser.

Immunoblotting
Cells grown to 80% density were washed with cold PBS before collection and lysis in protein lysis buffer (20 mM Tris HCl pH 8, 200 mM NaCl, 0.1% NP40, 2 mM $MgCl_2$, 2 mM EDTA, complete EDTA-free protease inhibitor cocktail: 1 tablet/50 ml lysis buffer, Roche #04693159001) on ice. Cell lysates were then sonicated for 30 min on ice and centrifuged for 15 min at 16,000 × g at 4 °C. Samples were then analyzed by Western blot; run on 8% SDS/PAGE, transferred to nitrocellulose membranes (Bio-Rad Laboratories,

Hercules, CA, USA), and blotted following manufacturer's recommendations with the indicated antibodies.

Patient-derived xenograft (PDX) development

Whole-exome sequencing analysis of 14-year-old patient's biopsy confirmed the presence of HEY1-NCoA2 gene fusion. The patient was clinically rediagnosed with MCS and underwent two surgeries, first for removal of primary tumor and second for distant metastasis in the pancreatic head. Written informed consent was acquired before the acquisition of both tumor samples by legal guardian. The study was approved by the institutional review board at the Cold Spring Harbor Laboratory (CSHL) and clinical institutions. The studies were conducted in accordance with recognized ethical guidelines (Declaration of Helsinki). Tumor specimens were cut into similar sizes and subcutaneously implanted into the dorsal region of ~6-week-old NOD/SCID/IL2λ-receptor null (NSG) anesthetized mice that were bred onsite at CSHL. The remaining tissue was either flash-frozen and stored in liquid nitrogen or fixed in 4% paraformaldehyde for 24 h for further histological analysis. When the tumors grew to 1–1.5 cm^3, they were resected, divided into equal pieces, and passaged into three NSG mice. The process was repeated to produce subsequent generations for drug testing and for maintenance.

The first passage (P) of the implanted tumor specimen (to six NSG mice) was abbreviated as P0. Subsequent subcutaneous PDX passages were conducted in the UV-clean laminar flow hood within at the CSHL animal surgery facility. In vivo tumor growth was monitored noninvasively by computed tomography (CT) imaging analysis.

Additional eight osteosarcoma PDX and eight conventional chondrosarcoma PDX tumors were obtained from the Jackson Laboratory (Farmington, CT, USA). All animal studies were performed in accordance with the policies of the Institutional Animal Care and Use Committee and were approved by the Institutional Review Board of CSHL.

PDXs drug treatment

PDX of MCS in passage P2 were used for drug treatment experiments, while PDX of osteosarcoma and chondrosarcoma were used 2 weeks after they arrived to the facility. PDX tumor measurements were taken by three-dimensional CT images before drug treatment. A suspension of imatinib (drug resuspended in corn oil and DMSO in 1:1 ratio, then diluted with PBS such that the final concentration of DMSO < 0.1%) was administered intraperitoneally twice daily, 50 mg/kg in each dose, for 17 days. The same administration regimen was used for the vehicle. Tumors were again analyzed by CT on the last day of treatment (17th day). After the last imaging, the mice were sacrificed and the tumors fixed in 4% paraformaldehyde for histological analysis. In this preclinical PDX study, 4 PDX of MCS primary tumors, 4 PDX of metastasis, 4 PDX of osteosarcoma, and 4 PDX of chondrosarcoma were used for each treatment (control and imatinib).

CT imaging of PDX mouse models

Whole-body 3D scans of PDX models were acquired by microCT (Mediso, Boston, MA, USA, nanoScan PET/CT) at an energy of 50 kVp and exposure of 186 μAs, with 480 projections per bed position. Tomographic images were reconstructed to an isotropic voxel size of 250 μm using a filtered back-projection algorithm with a high-resolution Ram-Lak filter. Interview Fusion software (Mediso) was used for CT image post processing and VivoQuant (Invicro) was used to manually segment tumors and measure tumor volume and mean density. Tumor mass was calculated by multiplying these two parameters. The significance of the increase or decrease in tumor volume and mass was assessed by a two-tailed Student's t test, with $p \leq 0.05$ considered significant.

Histology, IHC staining of tumor samples, and tissue microarray (TMA)

All tumor specimens were fixed in 4% paraformaldehyde for at least 24 h and up to 48 h prior to being embedded in paraffin blocks. Sections were then cut (4 μm) from each paraffin-embedded sample and mounted onto a slide followed by deparaffinization, rehydration, and staining. All IHC slides were stained with an automated slide stainer, Discovery Ultra automatic IHC stainer following standard protocols. After deparaffinization and rehydration, slides were subjected to antigen retrieval (Roche, Benchmark Ultra CC1) at 96 °C for 64 min; primary antibody was incubated at 37 °C for 1 h and Discovery multimer detection system (Roche, Discovery OmniMap HRP and Discovery ChromoMap DAB) was used to detect and amplify immunosignals. For negative controls, the primary antibodies were replaced by PBS. The polyclonal ABL1/2 antibody (MyBioSource, cat#MBS820417) was used at dilution of 1:50 in primary antibody dilution buffer (5% goat serum, 5% BSA, 0.5% triton X-100 in HBSS, pH 7.4). TMA (Biomax, Derwood, MD, USA, cat#OS803) and tumor tissue of PDX-primary tumor and PDX metastasis were all stained with the ABL1/2 antibody.

RESULTS

HPC expressing HEY1-NCoA2 show morphology changes and growth advantage

To obtain an in vitro model for MCS, we decided to introduce the HEY1-NCoA2 gene fusion into HPC (HEY1-NCoA2-HPC). We first aimed to find the most optimal growth conditions for HPC that would subsequently allow them to be transduced. As three different commercial media for culturing HPC were unsuccessful in keeping HPC cells alive beyond passages 7 and 10, we developed CIM, as described in the "Materials and methods" section. CIM together with optimized culturing conditions yielded higher viability of HPC, enhanced proliferation with shorter doubling times, and allowed us to culture HPC beyond passage 20 (Fig. 1a, b).

Next, the lentiviral transduction of HPC was performed to stably express the HEY1-NCoA2 gene fusion. The fusion was expressed together with the amino-terminal Flag-tag, while the carboxy-terminal traceable marker mVenus was expressed separately after the "self-cleaving" P2A sequence (Fig. 1c). As a control, we used a similar construct that only expressed eGFP under the same promoter (CMV). We were able to detect by western blotting the expression of HEY1-NCoA2 fusion using specific anti-Flag-tag, anti-NCoA2, and anti-HEY1 antibodies, all showing a band of 100 kDa apparent molecular weight (Fig. 1d, e). A specific shift from round to spindle-like morphology was detected in HEY1-NCoA2-HPC (Fig. 1f, g), resembling a feature of mesenchymal cells. In addition, HEY1-NCoA2-HPC presented a fitness advantage over their untransduced neighboring HPC as observed in a flow cytometry-based cell competition assay, where a 16% increase in mVenus positive cells was detected on day 8 after HEY1-NCoA2 fusion expression. This growth advantage was not observed in vector control (Vector-HPC) flow cytometry-based cell competition assay (Fig. 1h).

Single-cell RNA sequencing analysis of HEY1-NCoA2-HPC evidenced molecular features previously reported in MCS

To further characterize in vitro model of MCS, we performed sc-RNA sequencing of HPC and HEY1-NCoA2-HPC. UMAP analysis, a dimension-reduction and data visualization method, showed that untransduced HPC exhibit two different cell types grouped in two different clusters (Fig. 2a). Transduction of HPC with the HEY1-NCoA2 gene fusion results in a shift in gene expression that presents novel features, evidenced by the formation (or expansion) of a new cell cluster (Fig. 2a). Analysis of PuroR cassette expression clearly shows that the aforementioned cluster is mainly composed of transduced HPC (Fig. 2b). GSEA showed enrichment of cell division, downregulation of hallmark of apoptosis, and repression of negative regulation of cell population proliferation in HEY1-NCoA2-HPC (Fig. 2c), consistent with the cell growth advantage previously observed in competition assay (Fig. 1h). In addition, HEY1-NCoA2-HPC possesses a gene expression signature related to pediatric cancer markers, metastasis, genes involved in tumorigenesis of fusion-driven Ewing Sarcoma (EWSR1-FLI1 fusion), and upregulation of oncogenic MYC targets (Fig. 2c, d). Further, the HEY1-NCoA2-HPC population is enriched in the hedgehog signaling pathway (Hh), a critical positive regulator of HEY1 expression[29]. An upregulation in cisplatin response/XPC related genes and doxorubicin resistance genes, and down-regulation of serum/rapamycin-sensitive genes, was also observed in HEY1-NCoA2-HPC, which predicted the response of these cells to treatment with these drugs (Fig. 2c).
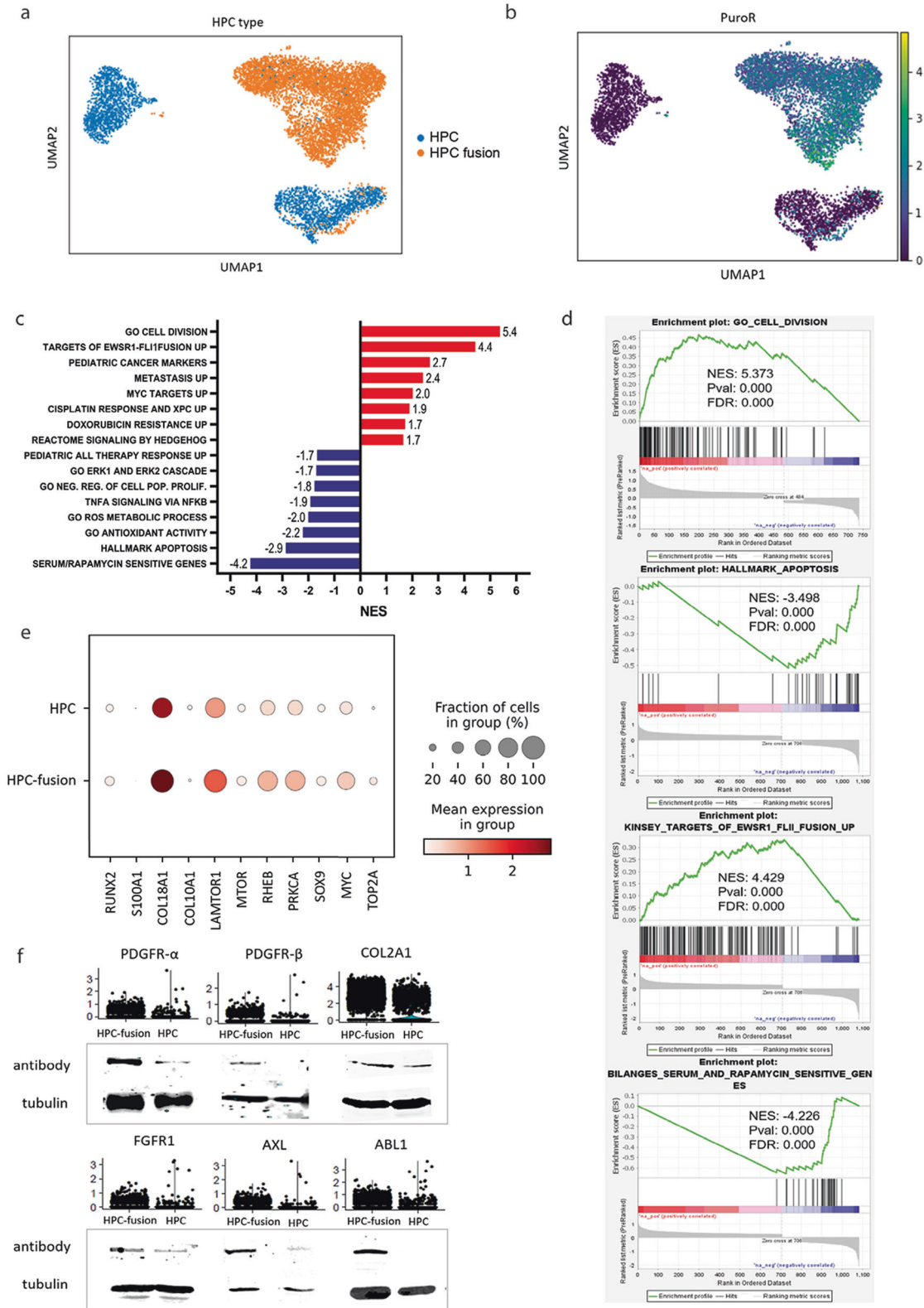
A dot plot analysis to visualize the expression status of specific genes that have a role in the terminal differentiation (hypertrophy) of chondrocytes (RUNX2, S100A1, COL10A1)[30,31], and genes related to pathways previously reported to be activated in MCS patient samples (SOX9, LAMTOR1, MTOR, RHEB, PRKCA)[25] is depicted in Fig. 2e. Hypertrophic markers presented a similar low expression pattern between HPC and HEY1-NCoA2-HPC, suggesting that the transduction did not cause terminal differentiation. In addition, the expression of collagen type II (COL2A1), a typical marker of articular chondrocytes, presented a high expression both at the mRNA and protein level (Fig. 2f), suggesting that transduced HPCs still retain features of healthy

Fig. 2 Single-cell RNA sequencing analysis of HEY1-NCoA2-HPC evidenced molecular features previously reported in mesenchymal chondrosarcoma. a UMAP analysis of HEY1-NCoA2-HPC and untransduced HPC showing three major clusters of all captured HPC single cells. **b** UMAP analysis depicting expression level of puromycin resistance cassette (PuroR). **c** GSEA analysis, showing enrichment of pathways between HEY1-NCoA2-HPC and untransduced HPCs. The chart represents the normalized enrichment score (NES) of selected significantly enriched GSEA GO-terms, pathways, and hallmarks (FDR $q < 0.01$). **d** GSEA enrichment plots of indicated gene sets. The normalized enrichment score (NES), P value (Pval), and the false discovery rates (FDR) are indicated for each gene set. **e** Accumulation of marker gene transcripts by cluster. The dot plot indicates the fraction of cells in each HPC or HEY1-NCoA2-HPC expressing a given marker (dot size) and the level of marker gene expression (dot intensity) for eight genes known to exhibit preferential expression in either HPC or MCS and 3 uniquely overexpressed genes found by GSEA. **f** Violin plots showing the single-cell expression distributions of distinct MCS markers (PDGFR-α, PDGFR-β, FGFR1), chondrogenic marker (COL2A1), and newly detected tyrosine kinases ABL1 and AXL with the corresponding antibody for Western Blot analysis and β-tubulin.

cartilage. The mTOR pathway was previously reported to be activated in MCS tissue samples[23]. At the RNA level, we were able to detect higher expression of LAMTOR1, a component of the Ragulator-Rag complex, in almost all HEY1-NCoA2-HPC, and Rheb in over 60% (Fig. 2e). Ragulator-Rag complex and Rheb are responsible for mTOR complex 1 (mTORC1) activation at the lysosomal surface under amino acid replete conditions[32]. The expression level of mTOR kinase was similar among HPC and HEY1-NCoA2-HPC, with a slightly larger percentage of HEY1-NCoA2-HPC expressing this gene. PKC-α (PRKCA) is another Ser/Thr kinase that is believed to be important for MCS, and presented a slightly higher expression level in over 80% of HEY1-NCoA2-HPC (Fig. 2e). Interestingly, oncogenic MYC was expressed at a higher level in over 60% of fusion-transduced HPC, while TOP2A was expressed in 20%. The Tyr kinases PDGFR-α, PDGFR-β, and FGFR3 were upregulated in HEY1-NCoA2-HPC both at the RNA and protein level (Fig. 2f), consistent with observations in MCS patient samples. Tyrosine kinases ABL1 and AXL were similarly upregulated, even though there were no previous reports on their involvement in MCS (Fig. 2f). As there are many clinically available drugs targeting ABL, we probed a TMA of several MCS samples and found that 60% of the samples presented a strong to moderate positivity for ABL1/2 mostly in the cell cytoplasm, suggesting that expression of ABL1/2 could be an additional feature of MCS (Fig. S1).

Fluorescence-based drug competition assay reveals selective sensitivity of HEY1-NCoA2-HPC to imatinib

We applied a fluorescence-based competition assay to screen for the efficacy and selectivity of drugs targeting HEY1-NCoA2-HPC. The presence of an effective and selective drug is evidenced by the percentage reduction of GFP+ (HEY1-NCoA2-HPC) cells, as measured by flow cytometry (Fig. 3). In addition, we measured a nonspecific cytotoxic effect of the drugs on "healthy" (untransduced) HPC as a percentage of remaining total cells relative to the number of untreated cells, measured by flow cytometry in each condition (Fig. 3).

Treatment with increasing concentrations of imatinib (0–15 µM) presented a strong and selective effect in reducing the HEY1-NCoA2-HPC population where the percentage of GFP+ cells significantly declined (Fig. 3b, c). No toxic effect was measured in untransduced HPC where the total number of cells remained unaffected (Fig. 3c). HPC transduced with the vector control were also unaffected by imatinib treatment (Fig. 3c, lower panel). Rapamycin (0–15 µM) did not present a selective effect on HEY1-NCoA2-HPC, but rather a nonspecific cytotoxic effect on all HPC, starting at concentrations as low as 1 µM, with a similar trend in HPC transduced with vector control (Fig. 3d). The increasing concentrations of the multikinase inhibitor regorafenib (0–15 µM), targeting VEGFR, FGFR, c-KIT, and PDGFR-β amongst others, showed a slight decrease in HEY1-NCoA2-HPC; however, the effect was not selective at concentrations above 5 µM as the total number of all cells drastically started to decline (Fig. 3e). Subsequently, we used specific inhibitors to identify the molecular pathways that could be involved in the sensitivity of HEY1-NCoA2-HPC to imatinib. We observed that

the PDGFR inhibitor CP-673451 presented a similar sensitivity profile to the one observed with the imatinib treatment (Fig. 3f). However, it also exhibited a stronger nonspecific cytotoxic effect at concentrations above 2 µM, also observed in HPC transduced with vector control (Fig. 3f, lower panel). The inhibition of the PDGFR downstream target JNK with the pan-JNK inhibitor (JNK-IN-8) did not show a strong selective effect and presented a high nonselective cytotoxicity starting at concentrations as low as 0.03 µM (Fig. 3g). Pan-FGFR inhibitor was also unsuccessful, in contrast to the effect observed in cells treated with regorafenib (Fig. 3h). The ABL-specific allosteric inhibitor Asciminib presented a similar trend to the one observed in PDGFR specific inhibitor, with a less toxic effect starting at the concentration of 3.5 µM (Fig. 3i). Finally, we tested the effect of commonly used chemotherapies, doxorubicin and cisplatin. Doxorubicin had a very strong nonselective effect on all cells starting at 2.5 µM, reaching over 80% of total death at 10 µM (Fig. 3j). This is expected because it has a nonselective mechanism of action. Strikingly, we detected a small number of HEY1-NCoA2-HPC that showed resistance to high concentrations of doxorubicin (16–25 µM). Cisplatin exhibited a similar nonspecific cytotoxic effect, starting at a concentration of 2 µM, with no evidence of resistance (Fig. 3k).

PDX mouse models of MCS primary tumor and metastasis are responsive to imatinib treatment

PDX models were also developed from MCS patient samples with clinically confirmed HEY1-NCoA2 gene fusion. The primary MCS tumor from the thoracic site and its pancreatic metastasis were subcutaneously implanted into the dorsal region of anesthetized 6-week-old NSGs (Fig. S2a, b). The growth of PDX tumors was tracked by CT imaging to measure subtle changes in tumor mass and volume. As we observed the positive ABL1/2 staining of MCS tumors in TMA (Fig. 1a–e), we also probed our PDX-metastasis model with an ABL1/2 antibody where strong positive staining was detected in all components of the biphasic growth pattern, with particularly strong staining of the cartilaginous component (Fig. S2c).

We utilized these newly generated preclinical models to investigate the in vivo efficacy of imatinib (Fig. S3a). Figure 4 represents the treatment of primary tumor PDX models with imatinib (Fig. 4b) and PDX treated with vehicle (Fig. 4a) where CT-imaging analysis revealed a significant decrease in volume (paired Student's t test, $p = 0.002$) and mass (paired Student's t test, $p = 0.0094$) in four imatinib-treated PDX tumors (Fig. 4c). Samples for histological analysis were taken on the last day of treatment (day 17), showing a dramatic loss of tumoral cells in lacunar space in imatinib-treated tumors but not in vehicle, indicating the cytotoxic effects of imatinib on the tumor's cellular components (Fig. 4d, e). The treatment of four PDX metastasis with imatinib and four with vehicle (Fig. 4f–j) showed a significant decrease in imatinib-treated tumors volume (paired Student's t test, $p < 0.0001$) and mass (paired Student's t test, $p < 0.0013$), also detected by CT imaging (Fig. 4g, h). On the cellular level, a large necrotic area surrounded by hemorrhagic boundaries and a dramatic loss of cellularity was observed by histological analysis (Fig. 4j). No drug-induced necrosis was observed in vehicle-treated tumors (Fig. 4i).
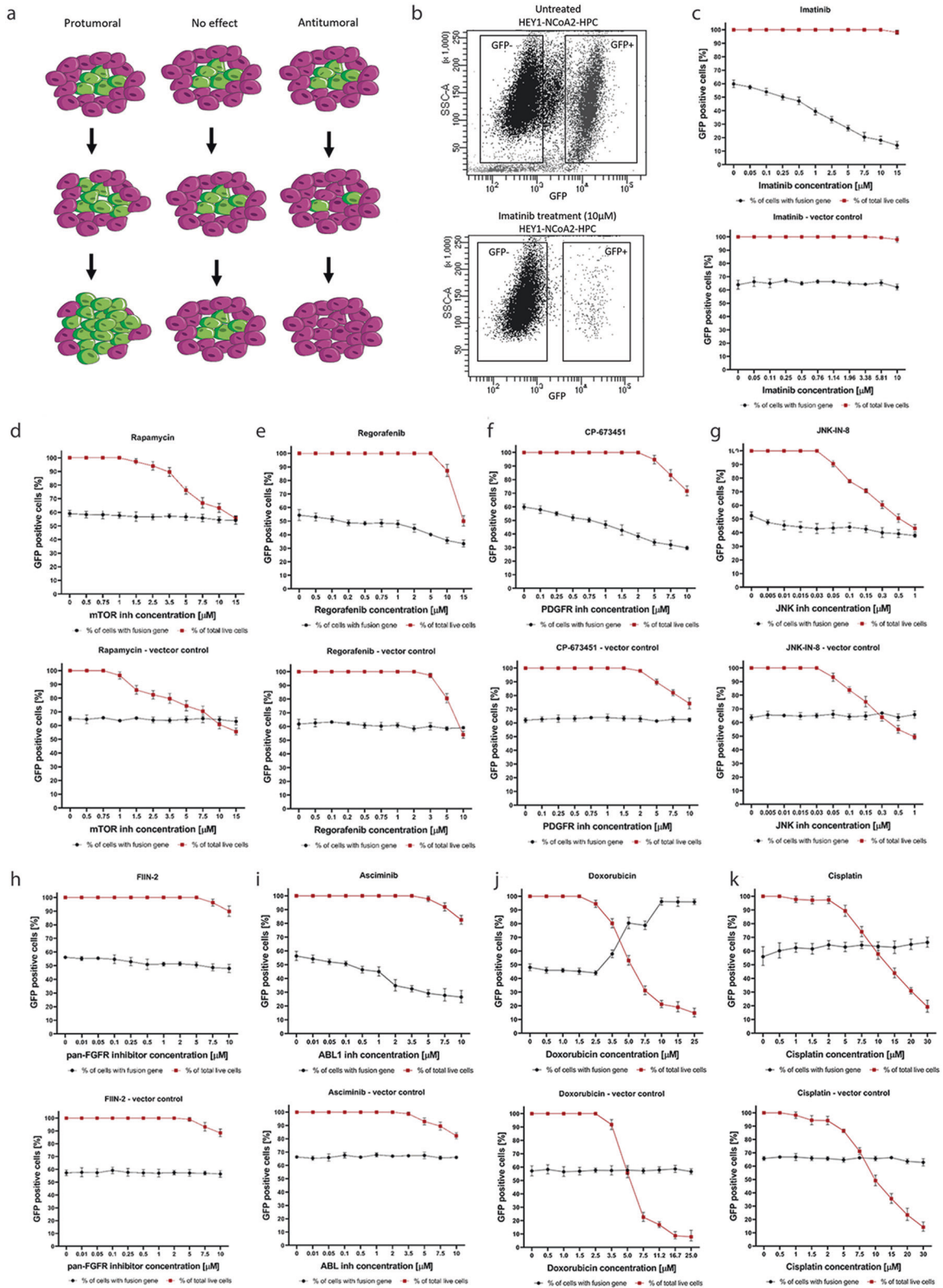
The preclinical study was extended to PDX models of other sarcomas, previously reported to be insensitive to imatinib treatment, such as conventional chondrosarcoma and osteosarcoma[27,33]. No significant changes in volume and mass of the tumors were observed by CT-imaging analysis (Fig. S4b, d). In addition, no significant treatment-related histological changes were observed (Fig. S4c, e).

DISCUSSION
Patients with rare cancers face many challenges including incorrect or late diagnosis, lack of clinical expertise, and inefficient treatment regimens[34]. Studies of common tumor types often have enough samples available to researchers to best ensure sufficient statistical power to address research hypotheses. However, in

Fig. 3 Fluorescence-based drug competition assay reveals selective sensitivity of HEY1-NCoA2-HPC to imatinib. a Scheme showing the basis of competition assay. The left panel shows either the protumoral effect or toxicity of the drug on untransduced HPC. The middle panel represents no effect of the drug on any cell population, while the right panel shows the antitumoral effect of the drug. This principle was tested on a mixed population of HPC and HEY1-NCoA2-HPC. **b** Fluorescence-activated cell sorting analysis dot plots showing the untreated mixed HPC and HEY1-NCoA2-HPC population (upper panel) and same population after 10 μM imatinib treatment for 3 days (lower panel). **c–e** The results of the drug competition assay using increasing concentrations of imatinib, rapamycin, or regorafenib (N = 5). **f–h** The results of the drug competition assay using an increasing concentration of specific inhibitors for PDGFR (**d**, N = 4), JNK (**e**, N = 3), FGFR (**f**, N = 5), and ABL1/2 (**g**, N = 5). **i–k** The results of the drug competition assay with an increasing concentration of doxorubicin or cisplatin (N = 5). The black line with circles represents the cytotoxicity of the drug to HEY1-NCoA2-HPC (or vector control), measured as a percentage of GFP+ cells, red line with squares represents the selectivity of the drug, measured as a percentage of a remaining total number of cells for each concentration.

studies of rare cancers, small sample sizes are inevitable, making it much harder to meet these criteria[35,36]. In this study, we developed an integrative platform for rare-cancer drug discovery, coupling the development of independent cellular and mouse models, a drug repurposing approach, and modern methodologies to find a more practical and efficient treatment strategy for MCS. MCS was first characterized almost 60 years ago, yet there are no available preclinical models, no deep molecular characterization, and no improved treatment options for over 20 years[9,37,38].

As MCS is thought to resemble the resting premesenchymal chondroprogenitors of the growth plate, arising either from undifferentiated chondroprogenitors, mature prehypertrophic-like chondrocytes, and/or osteoblastic-like chondrocytes, we reasoned that HPC would present a good cellular model for studying the impact of the HEY1-NCoA2 gene fusion[21]. It has been shown that the population of adult HPC consists of over seven different types of chondrocytes (including the ones mentioned above), thus providing a variety of cell subtypes to better recapitulate the environment where MCS arises[30,39]. The expansion and long-term culture of HPC in monolayer, however, have been very challenging in the past as HPC tend to become hypertrophic and lose their chondrogenic phenotype, eventually succumbing to cell death within the first 8 passages[31]. The improvement of HPC culturing conditions and the development of novel CIM media described here, allowed culturing of the HPC beyond passage 27. Transduced and untransduced HPC in passage 10 still exhibited a high rate of proliferation while expressing the chondrogenic markers (COL2A1, COL18A, SOX9), and little to no expression of hypertrophic markers (RUNX2, S100A,1 COL10A1) shown by RNA sequencing at a single-cell level. This signifies an important advancement for the use of HPC in future studies.

One of the hallmarks of tumor cells is increased cell fitness[40]. The ectopic expression of HEY1-NCoA2 gene fusion resulted in morphological changes (shifting to spindle-like shape), and increased cell fitness as detected by fluorescence competition assay. At the mRNA level, the GSEA correspondingly showed the enrichment of proliferation-related pathways, endorsing the gain of cell fitness in HPC expressing the fusion. Previously reported pathways in MCS such as mTOR, PKC-α, PDGFR-α, PDGRF-β, FGFR1, and SOX9[22,24,41] were also detected in single cells of HEY1-NCoA2-HPC at both, mRNA and protein levels. Strikingly, significant enrichment of tumor-related gene sets was mapped only to HEY1-NCoA2-HPC, namely pediatric cancer markers, MYC and EWSR1-FLI1 fusion target genes, and metastasis amongst others. Further research is needed to better understand the possible malignant transformation caused by the expression of HEY1-NCoA2 fusion in HPC.

Next, rather than embark on *de novo* drug discovery and development, we reasoned that a drug repurposing strategy would be a more efficient way to identify and implement new effective treatments for MCS. As the toxicity profile for approved therapies has already been established in Phase I clinical trials, these molecules can progress straight into Phase II for a new indication. We employed a highly sensitive and internally controlled drug screening assay for this purpose, based on

measuring cell fitness (cell competition assay) coupled with flow cytometry (percentage of GFP+ HPC) to measure the cytotoxic effects targeted specifically against HEY1-NCoA2-HPC[42]. Rapamycin (targeting mTORC1) was chosen based on previously reported strong IHC staining of MCS samples with specific antibodies against phospho-mTOR, phosphor-Akt, and phosphor-SK6. We identified overexpression of mTOR regulators (LAMTOR1 and RHEB) in the sc-RNA sequencing analysis of our developed in vitro model, however, no selective cytotoxic effect of rapamycin on HEY1-NCoA2-HPC was observed. Our GSEA analysis possibly predicted this, by showing strong downregulation of pathway M2328 in HEY1-NCoA2-HPC, composed of genes sensitive to rapamycin or serum depletion. This gene set comprises mainly ribosomal proteins whose translation is enhanced by activated mTORC1[43]. The fact that these genes are highly downregulated in HEY1-NCoA2-HPC on the mRNA level, could explain why inhibiting mTORC1 did not result in a strong selective cytotoxic effect towards HEY1-NCoA2-HPC. However, a Phase II clinical trial of rapamycin in MCS patients is currently being performed (NCT02821507), and the results will reveal whether the observations in the developed in vitro MCS model in this study reflect clinical observations.

The expression of FGFR1 and PDGFR-β at the mRNA and protein levels in HEY1-NCoA2-HPC model led to the decision to test the effect of licensed multikinase inhibitor regorafenib. Since an appreciable selective effect on HEY1-NCoA2-HPC was observed, we wanted to understand the contribution of overexpressed FGFR1. The selective pan-FGFR inhibitor did not show a selective cytotoxic response, however, indicating possibly less reliance on the FGFR pathway in MCS development.

Imatinib is a widely available inhibitor of tyrosine kinases such as PDGFR, KIT, and ABL, with a well-defined profile of toxicity. The use of imatinib in the management of MCS has been suggested by many previous studies[22,44,45]. PDGFR-α, PDGFR-β, and ABL were overexpressed in HEY1-NCoA2-HPC at mRNA and protein levels, therefore we wanted to test the efficacy of this drug in our in vitro model. Indeed, we observed a highly selective cytotoxic effect on HEY1-NCoA2-HPCs following imatinib treatment, with little to no effect on untransduced HPC. This result, in conjunction with our expression analyses, suggests that PDGFR signaling could play a central role in MCS. PDGFR-α, PDGFR-β, can contribute to the activation of additional pathways previously reported in MCS, such as PKC-α pathway via PLC-γ, and mTORC1 activation via phosphorylation of Akt[46,47]. To assess the contribution of PDGFR inhibition during imatinib treatment, we tested the efficacy of a pan-PDGFR inhibitor, which partially resembled the trend observed in the treatment with imatinib. These results suggest that PDGFR signaling is partially responsible for the selective effect on imatinib in this in vitro MCS model. ABL kinase is another imatinib target whose status in MCS was never assessed before. In HEY1-NCoA2-HPC the overexpression of ABL was detected at both, the mRNA and the protein levels. Moreover, the staining of MCS samples in TMA with ABL1/2 showed medium to high ABL expression. TMA samples have unknown HEY1-NCoA2 status, however, therefore, we tested allosteric ABL1/2 inhibitor Asciminib with our in vitro model. Surprisingly, a similar selective cytotoxic
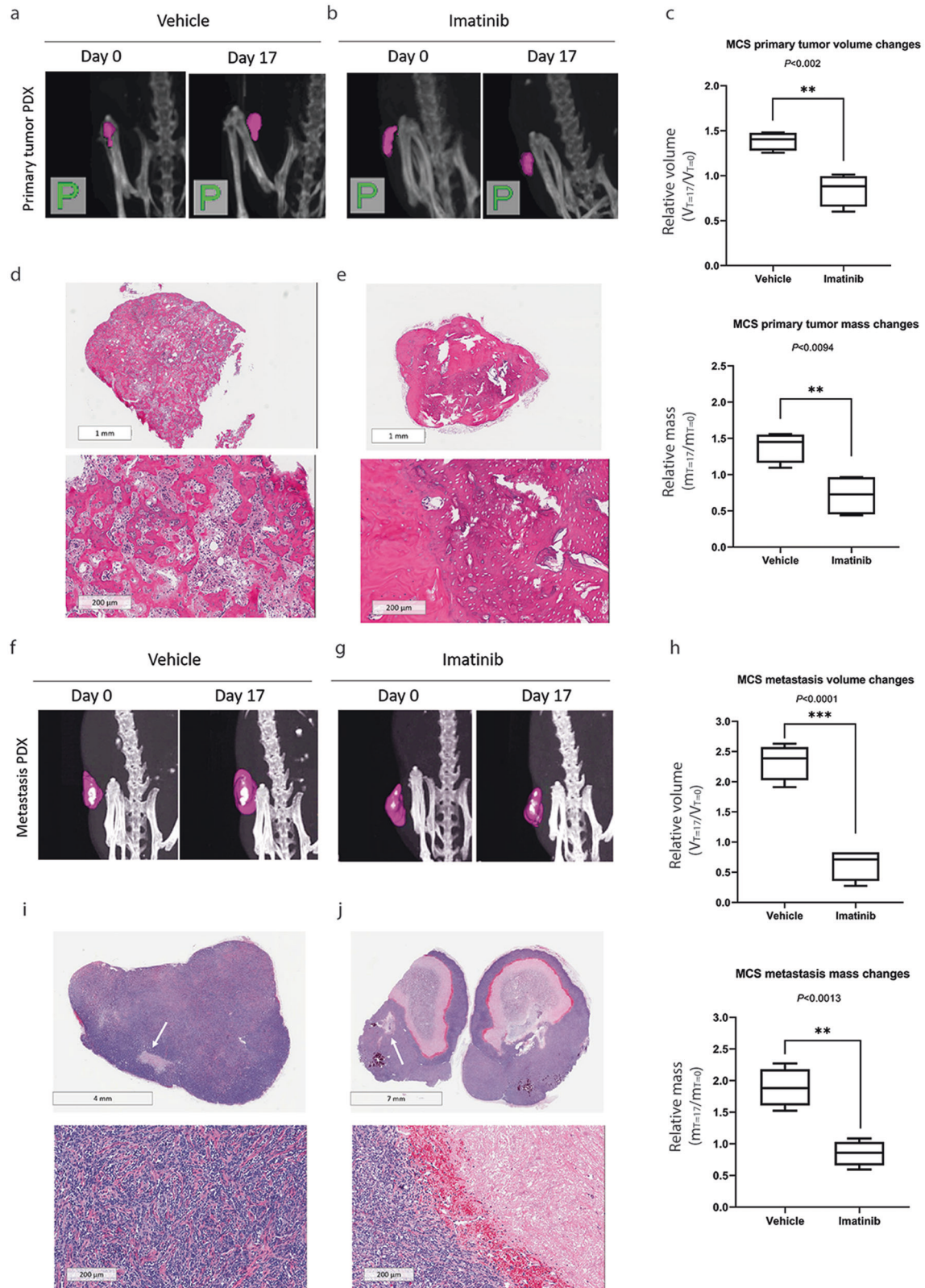
effect on HEY1-NCoA2-HPCs was detected, suggesting that ABL1/2 could be another important signaling pathway on MCS and possibly relevant to the imatinib treatment response. Previous studies have shown that ABL1 becomes activated following PDGF stimulation and is required for PDGF-induced endothelial-mesenchymal transition in tumors therefore a connection between these two pathways could be important for MCS development[48]. In addition, ABL was shown to phosphorylate the carboxy-terminus and activate the NCoA protein family, suggesting that potential phosphorylation of the HEY1-NCoA2

Fig. 4 The patient-derived xenograft mouse models of MCS primary tumor and MCS metastasis are responsive to imatinib treatment. a–e PDX of primary tumor treated with vehicle or imatinib. **f–j** PDX of MCS metastasis treated with vehicle or imatinib ($N = 4$). **a** A representative reconstructed 3D image of CT imaging of PDX-primary tumors treated with vehicle. The magenta color represents the cartilaginous component of the primary tumor. Down: H&E histological analysis of the PDX-primary tumor treated with vehicle. **b** A representative reconstructed 3D image of CT imaging of PDX-primary tumors treated with imatinib (up). The magenta color represents the cartilaginous component of the primary tumor. **c** The changes in tumor volume (up) (paired Student's t test, $p < 0.002$) and mass (down) (paired Student's t test, $p < 0.0094$), calculated by CT-imaging analysis ($N = 4$). **d** H&E histological analysis of the PDX-primary tumor treated with vehicle. **e** H&E histological analysis of the PDX-primary tumor treated with imatinib showing loss of cells in lacunar space. **f** A representative reconstructed 3D image of CT imaging of PDX metastasis treated with vehicle. The magenta color represents the cellular component of the tumor, white color shows the cartilaginous component. **g** A representative reconstructed 3D image of CT imaging of PDX metastasis treated with imatinib. The magenta color represents the cellular component of the tumor, white color shows the cartilaginous component. **h** The changes in tumor volume (paired Student's t test, $p < 0.0001$) and mass (paired Student's t test, $p < 0.0013$) were calculated by CT-imaging analysis ($N = 4$). **i** H&E histological analysis of the PDX-metastasis tumor treated with vehicle. A small area of spontaneous necrosis is shown with white arrows. **j** A large necrotic area surrounded by hemorrhagic boundaries and a dramatic loss of cellularity is shown with arrows in imatinib-treated tumors.

◀

fusion by ABL kinases could have a role in molecular reprogramming[49]. Taken together, the results from the use of specific ABL and PDGFR inhibitors may explain the strong imatinib effect observed in our HEY1-NCoA2-HPC model.

In addition to screening targeted therapies, we also tested commonly used chemotherapies for MCS management, doxorubicin, and cisplatin[8]. Doxorubicin treatment-induced over 70% of total cell death starting at a concentration of 7.5 μM, but a small population of HEY1-NCoA2-HPC was able to survive significantly higher doxorubicin doses, indicating a possible mechanism of drug resistance. Again, the GSEA analysis of sc-RNA sequencing of HEY1-NcoA2-HPC possibly predicted this resistance by showing the enrichment of doxorubicin resistance genes (M1037 pathway). In addition, high expression of oncogenic tyrosine kinase AXL in HEY1-NCoA2-HPC at both, mRNA and protein levels could contribute to doxorubicin and multiple-therapy resistance, as previously reported in other tumor cell types[50–52]. Given the fact that there are many controversial results about the efficacy of chemotherapy in MCS treatment and that over half of MCS patients experience late relapse[8–10,26], it is very important to further study the involvement of those genes in the possible mechanism of chemoresistance. In contrast, no similar resistance was observed when using cisplatin, neither in the cell competition assay nor in the GSEA analysis where cisplatin response genes were in fact upregulated.

PDX models are powerful tools in translational research for gaining a better understanding of possible conventional and novel drug treatment outcomes[53]. PDX models are extensively used in common cancer research but their availability is still very limited for rare cancers[27,53]. In this study, we report the first PDX models of HEY1-NCoA2 fusion-driven MCS of a primary tumor and its pancreatic metastasis, which will be important tools for future translational research. After treatment of both MCS-PDX models with imatinib for 17 days, a significant reduction in tumor mass and volume was measured by CT imaging. Further, histological analyses of tumors revealed substantial cell death in primary tumor and metastasis models on the last day of imatinib treatment. Overall, the observed efficacy of imatinib is very promising for the treatment of MCS tumors that express the HEY1-NCoA2 gene fusion.

Imatinib has previously been tested for the treatment of chondrosarcoma in Phase II clinical trial, where it failed to show a long-lasting effect on response and disease progression[33]. As chondrosarcoma subtypes are highly heterogeneous cartilage malignancies with contrasting clinical outcomes[54], a large molecular diversity between these subtypes coupled with a low incidence rate can increase the difficulty in identifying effective clinical treatments. Concordantly, we treated PDX models of conventional chondrosarcoma and osteosarcoma to investigate the effect of imatinib. Similar to clinical observations, we did not observe any effect of imatinib on tumor mass or volume reduction in both PDX models. These results suggest that imatinib is

specifically targeting MCS harboring the HEY1-NCoA2 fusion, in contrast to other chondrosarcomas and highlight the importance of proper diagnosis and identification of chondrosarcoma subtype, since prominent genetic differences, such as the expression of the HEY1-NCoA2 oncogenic fusion, can deeply impact the response to a specific treatment. In conclusion, our work rationally justifies a re-evaluation of clinically available imatinib to treat HEY1-NCoA2-driven MCS.

DATA AVAILABILITY
The datasets used and analyzed during the current study are available from the corresponding author on reasonable request.

REFERENCES
1. El Beaino, M. et al. Mesenchymal chondrosarcoma: a review with emphasis on its fusion-driven biology. *Curr. Oncol. Rep.* **20**, 37 (2018).
2. Ostlere, S. J., McDonald, B. & Athanasou, N. A. Mesenchymal chondrosarcoma associated with Goldenhar's syndrome. *Arch. Orthop. Trauma Surg.* **119**, 347–348 (1999).
3. Sadashiva, N. et al. Intracranial extraskeletal mesenchymal chondrosarcoma. *World Neurosurg.* **95**, 618.e611–618.e616 (2016).
4. Folpe, A. L. et al. Mesenchymal chondrosarcomas showing immunohistochemical evidence of rhabdomyoblastic differentiation: a potential diagnostic pitfall. *Hum. Pathol.* **77**, 28–34 (2018).
5. Wang, L. et al. Identification of a novel, recurrent HEY1-NCOA2 fusion in mesenchymal chondrosarcoma based on a genome-wide screen of exon-level expression data. *Genes Chromosomes Cancer* **51**, 127–139 (2012).
6. Hogendoorn, P. C. W., Bovee, J. M. & Nielsen, G. P. Chondrosarcoma (grades I-III), including primary and secondary variants and periosteal chondrosarcoma. In: *World Health Organization classification of tumours of soft tissue and bone*, (eds Fletcher, C. D. M., Bridge, J. A., Hogendoorn, P. C. W. & Mertens, F.) 4th edn, Vol. 5, p.264 (World Health Organization, IARC, Lyon, 2013).
7. Cesari, M. et al. Mesenchymal chondrosarcoma. an analysis of patients treated at a single institution. *Tumori J.* **93**, 423–427 (2007).
8. Xu, J., Li, D., Xie, L., Tang, S. & Guo, W. Mesenchymal chondrosarcoma of bone and soft tissue: a systematic review of 107 patients in the past 20 years. *PLoS ONE* **10**, e0122216 (2015).
9. Schneiderman, B. A., Kliethermes, S. A. & Nystrom, L. M. Survival in mesenchymal chondrosarcoma varies based on age and tumor location: a survival analysis of the SEER database. *Clin. Orthop. Relat. Res.* **475**, 799–805 (2017).
10. Frezza, A. M. et al. Mesenchymal chondrosarcoma: prognostic factors and outcome in 113 patients. A European Musculoskeletal Oncology Society study. *Eur. J. Cancer* **51**, 374–381 (2015).
11. Hilton, M. J. et al. Notch signaling maintains bone marrow mesenchymal progenitors by suppressing osteoblast differentiation. *Nat. Med.* **14**, 306–314 (2008).
12. Salie, R. et al. Ubiquitous overexpression of Hey1 transcription factor leads to osteopenia and chondrocyte hypertrophy in bone. *Bone* **46**, 680–694 (2010).
13. Xu, J. & Li, Q. Review of the in vivo functions of the p160 steroid receptor coactivator family. *Mol. Endocrinol.* **17**, 1681–1692 (2003).
14. Spencer, T. E. et al. Steroid receptor coactivator-1 is a histone acetyltransferase. *Nature* **389**, 194–198 (1997).
15. Yin, H., Glass, J. & Blanchard, K. L. MOZ-TIF2 repression of nuclear receptor-mediated transcription requires multiple domains in MOZ and in the CID domain of TIF2. *Mol. Cancer* **6**, 51 (2007).

P. Safaric Tepes et al.

16. Yoshida, H. et al. PAX3-NCOA2 fusion gene has a dual role in promoting the proliferation and inhibiting the myogenic differentiation of rhabdomyosarcoma cells. *Oncogene* **33**, 5601–5608 (2014).

17. Xiao, X., Garbutt, C. C., Hornicek, F., Guo, Z. & Duan, Z. Advances in chromosomal translocations and fusion genes in sarcomas and potential therapeutic applications. *Cancer Treat. Rev.* **63**, 61–70 (2018).

18. Hagenbuchner, J. & Ausserlechner, M. J. Targeting transcription factors by small compounds—current strategies and future implications. *Biochem. Pharmacol.* **107**, 1–13 (2016).

19. Karlsson, E., Lindberg, A., Andersson, E. & Jemth, P. High affinity between CREBBP/p300 and NCOA evolved in vertebrates. *Protein Sci.* **29**, 1687–1691 (2020).

20. Keppel, T. R., Howard, B. A. & Weis, D. D. Mapping unstructured regions and synergistic folding in intrinsically disordered proteins with amide H/D exchange mass spectrometry. *Biochemistry* **50**, 8722–8732 (2011).

21. Aigner, T. et al. Cell differentiation and matrix gene expression in mesenchymal chondrosarcomas. *Am. J. Pathol.* **156**, 1327–1335 (2000).

22. Brown, R. E. & Boyle, J. L. Mesenchymal chondrosarcoma: molecular characterization by a proteomic approach, with morphogenic and therapeutic implications. *Ann. Clin. Lab. Sci.* **33**, 131–141 (2003).

23. Brown, R. E. Morphoproteomic portrait of the mTOR pathway in mesenchymal chondrosarcoma. *Ann. Clin. Lab. Sci.* **34**, 397–399 (2004).

24. van Oosterwijk, J. G. et al. Screening for potential targets for therapy in mesenchymal, clear cell, and dedifferentiated chondrosarcoma reveals Bcl-2 family members and TGFbeta as potential targets. *Am. J. Pathol.* **182**, 1347–1356 (2013).

25. Wehrli, B. M., Huang, W., De Crombrugghe, B., Ayala, A. G. & Czerniak, B. Sox9, a master regulator of chondrogenesis, distinguishes mesenchymal chondrosarcoma from other small blue round cell tumors. *Hum. Pathol.* **34**, 263–269 (2003).

26. de Jong, Y. et al. Inhibition of Bcl-2 family members sensitizes mesenchymal chondrosarcoma to conventional chemotherapy: report on a novel mesenchymal chondrosarcoma cell line. *Lab. Investig.* **96**, 1128–1137 (2016).

27. Sharifnia, T., Hong, A. L., Painter, C. A. & Boehm, J. S. Emerging opportunities for target discovery in rare cancers. *Cell Chem. Biol.* **24**, 1075–1091 (2017).

28. Wolf, F. A., Angerer, P. & Theis, F. J. SCANPY: large-scale single-cell gene expression data analysis. *Genome Biol.* **19**, 15 (2018).

29. Benito-Gonzalez, A. & Doetzlhofer, A. Hey1 and Hey2 control the spatial and temporal pattern of mammalian auditory hair cell differentiation downstream of Hedgehog signaling. *J. Neurosci.* **34**, 12865–12876 (2014).

30. Ji, Q. et al. Single-cell RNA-seq analysis reveals the progression of human osteoarthritis. *Ann. Rheum. Dis.* **78**, 100–110 (2019).

31. Carluccio, S. et al. Progenitor cells activated by platelet lysate in human articular cartilage as a tool for future cartilage engineering and reparative strategies. *Cells* **9**, 1052 (2020).

32. Liu, G. Y. & Sabatini, D. M. mTOR at the nexus of nutrition, growth, ageing and disease. *Nat. Rev. Mol. Cell Biol.* **21**, 183–203 (2020).

33. Grignani, G. et al. A phase 2 trial of imatinib mesylate in patients with recurrent nonresectable chondrosarcomas expressing platelet-derived growth factor receptor-alpha or -beta: an Italian Sarcoma Group study. *Cancer* **117**, 826–831 (2011).

34. Pillai, R. K. & Jayasree, K. Rare cancers: challenges & issues. *Indian J. Med. Res.* **145**, 17–27 (2017).

35. Mitani, A. A. & Haneuse, S. Small data challenges of studying rare diseases. *JAMA Netw. Open* **3**, e201965 (2020).

36. Alvi, M. A., Wilson, R. H. & Salto-Tellez, M. Rare cancers: the greatest inequality in cancer research and oncology treatment. *Br. J. Cancer* **117**, 1255–1257 (2017).

37. Nakashima, Y., Unni, K. K., Shives, T. C., Swee, R. G. & Dahlin, D. C. Mesenchymal chondrosarcoma of bone and soft tissue. A review of 111 cases. *Cancer* **57**, 2444–2453 (1986).

38. Dahlin, D. C. & Henderson, E. D. Mesenchymal chondrosarcoma. Further observations on a new entity. *Cancer* **15**, 410–417 (1962).

39. Wang, X. et al. Comparison of the major cell populations among osteoarthritis, Kashin-Beck disease and healthy chondrocytes by single-cell RNA-seq analysis. *Cell Death Dis.* **12**, 551 (2021).

40. Colom, B. et al. Mutant clones in normal epithelium outcompete and eliminate emerging tumours. *Nature* **598**, 510–514 (2021).

41. Muller, S., Soder, S., Oliveira, A. M., Inwards, C. Y. & Aigner, T. Type II collagen as specific marker for mesenchymal chondrosarcomas compared to other small cell sarcomas of the skeleton. *Mod. Pathol.* **18**, 1088–1094 (2005).

42. Eekels, J. J. et al. A competitive cell growth assay for the detection of subtle effects of gene transduction on cell proliferation. *Gene Ther.* **19**, 1058–1064 (2012).

43. Bilanges, B. et al. Tuberous sclerosis complex proteins 1 and 2 control serum-dependent translation in a TOP-dependent and -independent manner. *Mol. Cell Biol.* **27**, 5746–5764 (2007).

44. Shakked, R. J., Geller, D. S., Gorlick, R. & Dorfman, H. D. Mesenchymal chondrosarcoma: clinicopathologic study of 20 cases. *Arch. Pathol. Lab. Med.* **136**, 61–75 (2012).

45. Guo, J. et al. A case of mesenchymal chondrosarcoma arising from the femoral vein with 8 years of follow-up. *Ann. Vasc. Surg.* **29**, 1455 e1451–1455 e1455 (2015).

46. Zhang, H. et al. PDGFRs are critical for PI3K/Akt activation and negatively regulated by mTOR. *J. Clin. Investig.* **117**, 730–738 (2007).

47. Ho, A. L. et al. PDGF receptor alpha is an alternative mediator of rapamycin-induced Akt activation: implications for combination targeted therapy of synovial sarcoma. *Cancer Res.* **72**, 4515–4525 (2012).

48. Yang, L., Lin, C. & Liu, Z. R. P68 RNA helicase mediates PDGF-induced epithelial mesenchymal transition by displacing Axin from beta-catenin. *Cell* **127**, 139–155 (2006).

49. Oh, A. S. et al. Tyrosine phosphorylation of the nuclear receptor coactivator AIB1/SRC-3 is enhanced by Abl kinase and is required for its activity in cancer cells. *Mol. Cell Biol.* **28**, 6580–6593 (2008).

50. Wang, C. et al. Gas6/Axl axis contributes to chemoresistance and metastasis in breast cancer through Akt/GSK-3beta/beta-catenin signaling. *Theranostics* **6**, 1205–1219 (2016).

51. Abdel-Rahman, W. M., Al-Khayyal, N. A., Nair, V. A., Aravind, S. R. & Saber-Ayad, M. Role of AXL in invasion and drug resistance of colon and breast cancer cells and its association with p53 alterations. *World J. Gastroenterol.* **23**, 3440–3448 (2017).

52. Tepes, P. S., et al. An epigenetic switch regulates the ontogeny of AXL-positive/EGFR-TKi-resistant cells by modulating miR-335 expression. Elife **10**, e66109 (2021).

53. Yoshida, G. J. Applications of patient-derived tumor xenograft models and tumor organoids. *J. Hematol. Oncol.* **13**, 4 (2020).

54. Nicolle, R. et al. Integrated molecular characterization of chondrosarcoma reveals critical determinants of disease progression. *Nat. Commun.* **10**, 4622 (2019).

AUTHOR CONTRIBUTIONS

P.S.T. contributed to the study design, conceptualization, data collection and curation, interpretation, methodology, formal analysis, funding acquisition, writing original draft, and editing. D.S. contributed to the formal analysis, data curation, interpretation, writing original draft, critical review, and editing. S.J. contributed to single-cell sequencing data analysis and interpretation, critical review, and editing of the final draft. D.R. contributed to histological analysis and data curation. S.K.L. contributed to the CT scan-related data collection and curation, formal analysis, and critical review and editing of the original draft. R.S. contributed to study design, conceptualization, writing the original draft, and funding acquisition.

FUNDING INFORMATION

COMPETING INTERESTS

The authors declare no competing interests.

ETHICS APPROVAL AND CONSENT TO PARTICIPATE

The study was approved by the institutional review board at the CSHL. All animal experiments were performed following the National Research Council's Guide for the Care and Use of Laboratory Animals. Protocols were approved by the CSHL Animal Care and Use Committee (933922-1 Development of mouse models—integrated protocols). The studies were conducted following recognized ethical guidelines (Declaration of Helsinki).

ADDITIONAL INFORMATION

Supplementary information The online version contains supplementary material available at https://doi.org/10.1038/s41374-021-00704-4.

Correspondence and requests for materials should be addressed to Polona Safaric Tepes.

Reprints and permission information is available at http://www.nature.com/reprints

Publisher's note Springer Nature remains neutral with regard to jurisdictional claims in published maps and institutional affiliations.

SPRINGER NATURE